(Received 1 January 2025, Accepted 8 April 2025, Scheduled 29 April 2025)

Optimization Design of Axial Flux Permanent Magnet Synchronous Motor Based on Multi-Objective Genetic Algorithm

Huijun Liu[1, 2, *]

[1] College of Mechanical and Electrical Engineering
Zhumadian Vocational and Technical College, Zhumadian 463000, China
[2] Henan Intelligent Sorting Technology Application Engineering Research Center
Zhumadian Vocational and Technical College, Zhumadian 463000, China

ABSTRACT: As a new type of motor, axial flux permanent magnet synchronous motor has the advantages of compact structure and high power density. It shows good application prospects in new energy vehicles, unmanned aerial vehicles, and other fields. However, axial flux permanent magnet synchronous motor needs to consider the balance of multiple objectives during the design process, which makes its optimal design a complex multi-objective optimization problem. Therefore, the study proposes a motor optimization method based on multi-objective genetic algorithm. The method optimizes the rotor and stator parameters of the motor by establishing an analytical model of the motor's magnetic field and combining it with a multi-objective genetic algorithm. The experimental results indicated that the optimized motor with multi-objective genetic algorithm reached 92% in terms of efficiency, 25% in terms of power density; energy consumption was reduced to 2.5 kWh; failure rate was reduced to 1.5%; and noise level was reduced to 65 dB. In addition, the multi-objective genetic algorithm significantly improved the control stability index, which increased to 98%, indicating a more stable motor response under varying loads. The disturbance rejection capability was enhanced to 99%, demonstrating strong resistance to external noise and parameter fluctuations. Furthermore, the system response frequency reached 100 Hz, reflecting a faster dynamic response to input variations. It is indicated that the optimization method based on multi-objective genetic algorithm can effectively enhance the comprehensive performance of axial flux permanent magnet synchronous motor and significantly improve its competitiveness in high power density and high efficiency applications.

1. INTRODUCTION

As energy consumption and environmental issues become more serious, electric motors are increasingly valued for their high efficiency, energy savings, and environmental friendliness as key driving devices in industry and transportation. The traditional radial flux permanent magnet motor (RFPMM) has long dominated the mainstream market due to its mature design and wide range of applications. However, with the increasing demands on motor performance, especially in terms of power density (PD), size, and efficiency, axial flux permanent magnet synchronous motor (AFPMSM) is gradually becoming a strong candidate to replace the traditional RFPMM [1]. Compared to conventional motors, AFPMSMs have a higher PD and a more compact structure, and their unique axial flux path enables motors to realize more power in a smaller volume, especially at low speed and high torque conditions, providing significant advantages. One of the key advantages of axial flux motors is their compactness and efficient heat dissipation [2]. Since the magnetic flux of a motor flows in the axial direction, the rotor and stator are arranged in the axial direction, which reduces the axial dimensions of the motor. Compared to conventional motors, AFPMSMs can provide higher PD in a smaller space for applications with stringent size requirements. The axial arrangement allows the air flow to contact the rotor and stator more directly, which improves the cooling effect of the motor and makes it suitable for long-term, high-load operation. However, AFPMSMs must balance multiple objectives such as PD, efficiency, thermal management, and structural stability during the design process. This makes their optimal design a complex multi-objective optimization (MOO) problem. AFPMSMs are widely used in industrial automation, electric vehicles, and robotics due to their high PD, high energy efficiency, and good dynamic response characteristics. Zhao et al. presented a retrospective review in an attempt to facilitate a comprehensive study of AFPMSMs. The article firstly introduced the basic topology of AFPMSM and summarized the key points of design and control optimization. It was revealed that the current state of development of efficiency-optimized control strategies outlined problem-specific control strategies and discussed the current difficulties and trends faced [3]. To increase the resilience and fault-tolerance of a six-phase AFPMSM in power generation, Bouyahia et al. proposed a real-time fault-tolerant approach based on a fuzzy logic controller. The results showed that the strategy was independent of the system model and effective in dealing with model disturbances and parameter vari-

* Corresponding author: Huijun Liu (lhjhpu@163.com).

ations. Compared with the classical proportional-integral (PI) controller, it showed higher efficiency and robustness under both health and fault conditions [4]. Jiang et al. proposed a modulation method to optimize the sliding clamping strategy of a five-phase open-wound permanent magnet synchronous motor (PMSM) driven by dual inverters and to reduce the effect of harmonic voltages on the motor performance. The results showed that the method effectively avoided the introduction of additional harmonic components by limiting the reference voltage of the clamping inverter and sliding it in both directions. Its effectiveness on resistive inductive loads and five-phase open-winding PMSMs was experimentally verified [5]. To increase the resilience of PMSM drives to parameter uncertainties and load disturbances in electric vehicle applications, Bhattacharjee et al. proposed a sophisticated deep reinforcement learning-based speed and current control method. The results showed that the method effectively mitigated the disturbances caused by parameter variations and load torque. Its performance was also verified by real-time software in-loop tests, demonstrating its superiority over adaptive proportional-integral control [6].

Tasoglu and Ilgin proposed a simulation-based genetic algorithm (GA) method to simultaneously optimize the reverse logistics network design, disassembly line balancing, and disassembly sequencing problems. The results of the study showed that the method could achieve lower total cost of ownership and improve process efficiency and customer satisfaction through joint optimization and sequencing decisions [7]. Kumar et al. proposed a hybrid GA and simulated annealing approach to strategically determine the best location for plug-in electric vehicle (PEV) charging stations in an effort to seamlessly integrate them into a distribution grid with distributed photovoltaic systems. The results showed that the method reduced power losses, maintained acceptable voltage levels, and improved the sustainability and reliability of the distribution grid [8]. Shen et al. developed an optimization-based model and proposed an active tensioned string beam structure to achieve active control of the deflection of a beam string structure. The results of the study showed that the integration of the hybrid GA control system with a back-propagation neural network successfully reduced the deflection response by at least 80%. The effectiveness and precision of the control framework were confirmed by optimizing the internal forces of the beam and achieving a maximum reduction in stress response about 60% [9].

In summary, there are numerous researchers who have applied various optimization algorithms to optimize the design of AFPMSMs and achieved remarkable results. However, there are still some challenges in MOO and handling complex parameter spaces, especially when the optimization effect is limited when considering multiple performance metrics. Therefore, this study proposes a multi-objective GA approach for the optimal design of AFPMSMs by analytically modeling the motor magnetic field (MF) and combining it with GA for global search and optimization of motor parameters. The innovation of the study is the use of multi-objective GA to optimize AFPMSM. It comprehensively optimizes several key performance indexes, such as PD, efficiency, temperature rise, and torque output. The design accuracy is improved by accurate analytical modeling of the MF. The study provides new design ideas and theoretical support for the engineering application of electric motors and enhances the feasibility of applying AFPMSM technology in new energy vehicles and other high-performance applications.

2. METHODS

The first subsection establishes the AFPMSM MF analytical modeling. The second subsection addresses the problem of MOO and uses GA to find the optimality of each objective.

2.1. Analytical Modeling of the AFPMSM Magnetic Field

AFPMSM is a newer type of PMSM with an axial flux path. It has a compact structure and high PD compared to conventional RFPMMs. Its rotor and stator are designed to be arranged along the axial direction, which makes the motor smaller and suitable for space-constrained applications [10, 11]. Motor topology refers to the layout and connection of the components inside the motor, and different topologies determine the operating principle and performance characteristics of the motor. The main feature of the topology of an AFPMSM is that the magnetic flux flows along the axial direction of the motor, and the rotor and stator arrangements are aligned along the axial direction. The rotor of an AFPMSM is usually composed of permanent magnet (PM) material, which generates electric potential to drive the load through the interaction of the MF with stator windings [12, 13]. When the analytical model of the motor is built, the three-dimensional structure AFPMSM needs to be expanded along the radius to be equivalent to a two-dimensional linear motor. The structure is shown in Fig. 1.

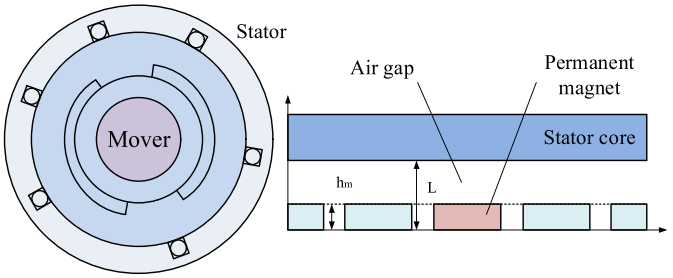

FIGURE 1. 2D equivalent model of motor no-load magnetic field.

In Fig. 1, the three-dimensional structure of the AFPMSM is expanded into a two-dimensional model, and it can be assumed that the magnetic flux flows along the axial direction of the motor, while the relative motions of the stator and rotor can be described by a two-dimensional plane model. In practical analysis, it can be assumed that the MF is uniformly distributed in the axial direction or behaves in the form of plane wave propagation in some specific regions [14, 15]. Since the flux direction of an axial flux motor is the same as the axial direction of the motor, when equating it to a two-dimensional linear motor, it can be assumed that the MF and current distribution of the motor are analyzed in a two-dimensional plane. The expression for the magnetic flux density (MFD) at the motor air gap (AG) is shown in Equation (1).

$$B_1 = \mu_0 H_1 \tag{1}$$

According to this equation, B_1 denotes the MFD at the AG of the motor. B_1 denotes the MF strength in the AG region. μ_0 denotes the vacuum permeability. The expression of MFD at the PM is shown in Equation (2).

$$B_2 = B_r + \mu H_2 = \mu_0 M + \mu_0 \mu_r H_2 \tag{2}$$

Let B_2 denote the MFD at the PM, H_2 the MF strength in the region of the PM, and M the magnetization strength of the PM. The magnetization strength of the PM is shown in Equation (3).

$$M_y(x) = \sum_{\infty}^{n=1,3,5\ldots} M_n \cos(u_n x) \tag{3}$$

From Equation (3), n can be expressed as the number of spatial harmonics of the MF; M_n can be expressed as the coefficient of each term in the level, which represents the components of the magnetization intensity of each order; u_n can be expressed as the coefficient of variation of the magnetization strength in space. Considering stator slotting, the expression of AG flux density at no load of the motor is shown in Equation (4).

$$\begin{cases} B_{xs} = B_{x_1}\mathrm{Re}(\lambda) - B_{y_1}\mathrm{Im}(\lambda) \\ B_{ys} = B_{y_1}\mathrm{Re}(\lambda) + B_{x_1}\mathrm{Im}(\lambda) \end{cases} \tag{4}$$

In the above equation, B_x and B_y are the components of the MFD in the AG in x and y directions. The real and imaginary components are represented by $\mathrm{Re}(\lambda)$ and $\mathrm{Im}(\lambda)$, respectively.

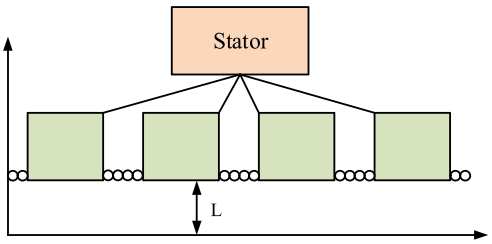

FIGURE 2. Structure of two-dimensional equivalent model of motor armature reaction magnetic field.

In Fig. 2, in a motor, the armature windings are located in the stator slots. Due to the complex distribution of the windings, the problem of calculating the armature reactive MF is often simplified by equating the windings to current sheets uniformly distributed in the slots. In this way, the current density of the armature can be approximated as uniformly distributed in a two-dimensional plane [16]. In this simplified model, the current sheet is assumed to be uniformly distributed in a plane of the stator. This plane is usually parallel to the axial direction of the motor, so the distribution of the armature reactive MF can be described by a two-dimensional planar model. The current distribution of the current sheet usually takes into account the current-carrying situation of the motor, such as DC current or AC current. In a two-dimensional model, the MF generated by the current sheet can then be described by a MF source model. The stator three-phase winding currents of the motor are shown in Equation (5).

$$\begin{cases} i_{\mathrm{A}} = \sum_{\infty}^{k} I_k \sin(k2\pi f t) \\ i_{\mathrm{B}} = \sum_{\infty}^{k} I_k \sin\left[k(2\pi f t - 2\pi/3)\right] \\ i_{\mathrm{C}} = \sum_{\infty}^{k} I_k \sin\left[k(2\pi f t + 2\pi/3)\right] \end{cases} \tag{5}$$

From Equation (5), i_{A}, i_{B}, and i_{C} represent the A, B, and C phase currents, respectively; I_k is the amplitude of the kth harmonic; f is the operating frequency of the motor; t is the time; k is the serial number of the harmonic. When the motor rotor rotates, the MF generated by the PMs cuts through the stator windings, thereby inducing an electromotive force in accordance with Faraday's law of electromagnetic induction. The reverse electromotive force, or voltage, is induced in the stator winding in accordance with Faraday's law of electromagnetic induction [17]. Under no-load conditions, no current flows in the stator windings, so the induced voltage is caused entirely by the rotor motion and is called the no-load back electromotive force. The distribution of the unit motor windings is shown in Fig. 3.

In Fig. 3, this image shows a two-dimensional planar cross-section of a three-phase PMSM. The blue-green region in the center is the stator and contains multiple slots. Each slot is embedded with a rectangle of a different color to represent the armature windings. The windings are labeled as "C+", "C−", "A+", "A−", "B+", "B−", corresponding to the positive and negative polarities of the three-phase winding, and is periodically arranged. The expression for the reverse electromotive force is shown in Equation (6).

$$E = k_e \cdot \omega \tag{6}$$

In the above equation, k_e is the reverse electromotive force constant, ω the rotor mechanical angular velocity, and E the counter electromotive force, which is directly related to the electromagnetic characteristics of the motor.

2.2. Optimization Study of AFPMSM Based on Multi-Objective GA

After building the analytical model of AFPMSM MF, its parameters are optimized by GA. The GA used in the study is an improved version of the classic GA. Unlike traditional genetic algorithms that use standard fitness functions and crossover mutation processes, this algorithm introduces adaptive mutation rates and dynamic selection pressure to improve convergence speed and avoid local optima. The core modifications are as follows: firstly, the adaptive mutation probability changes with the iteration process; secondly, a mixed selection strategy integrates tournament selection and ranking based selection; and finally, an elite retention mechanism retains high-performance individuals to enhance global search capabilities. These improvements make the proposed genetic algorithm more suitable for solving multi-objective optimization problems in AFPMSM. The GA deals with candidate solutions in the form of populations, each of which is called an

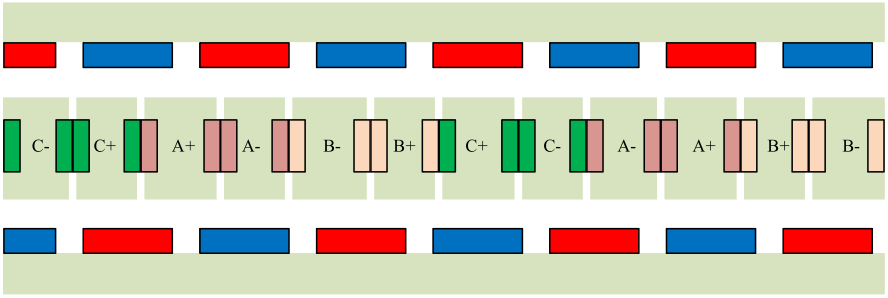

FIGURE 3. Distribution of unit motor windings.

"individual" and is represented by a code. The algorithm approximates the optimal solution step by step by simulating the genetic, selection, crossover, and mutation operations of biological evolution. In the optimization process, it is necessary to first clarify the key motor design parameters and their initial values to ensure that the optimization algorithm can effectively search for the optimal solution. The selected parameters include permanent magnet thickness (2.5–8.0 mm), rotor outer layer thickness (1.0–5.0 mm), stator slot height (5.0–15.0 mm), stator tooth width (2.0–10.0 mm), air gap length (0.5–2.5 mm), and stator slot width (2.5–8.0 mm). For parameter adjustment in the optimization process, adaptive mutation probability is first adopted, with an initial mutation probability set at 0.1, gradually decreasing with increasing iteration times to avoid premature convergence problems. Secondly, adopting an elite retention strategy, the top 5% of individuals with the highest fitness are retained in each generation to ensure that excellent solutions are not eliminated. In terms of crossover operator selection, combining single point crossover and uniform crossover, the initial crossover probability is set to 0.9 and reduced in the later stage to improve local search ability. In addition, a constraint violation penalty function is introduced to reduce the fitness of solutions that exceed the set limit, in order to ensure that the final result meets engineering constraints. The structure of the algorithm is shown in Fig. 4.

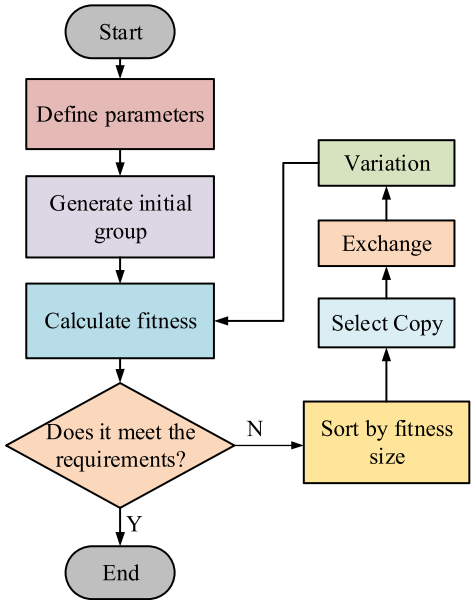

FIGURE 4. GA flow.

In Fig. 4, first, the algorithm starts by encoding the parameter set. After initializing the population, a predetermined number of potential solutions are chosen at random to serve as the initial individuals. After that, it moves on to the adaptation evaluation phase, which determines each person's adaptation value based on the objective function, taking into account both their strengths and weaknesses. After the evaluation is completed, the algorithm determines whether the stopping rule is satisfied. If the stopping condition is not satisfied, genetic operations are performed, including selection, crossover, and mutation. Based on fitness, selection is the process of choosing the best individuals from the population to reproduce. To increase the diversity of the population, crossover is the process of creating new individuals by combining some of the genes of two individuals. Mutation is the random alteration of certain genes to avoid falling into a local optimum. After generating a new generation of population through genetic manipulation, it returns to the evaluation phase, forming an iterative loop. If the stopping condition is satisfied, the algorithm ends, and the final optimized solution or optimal individual is output. MOO is a class of optimization problems that simultaneously optimize multiple objective functions. GA is the foundation of the study, which aims to optimize the AFPMSM design.

In Fig. 5, first, the design requirements and optimization objectives are determined, and the parameters and objective functions to be optimized are specified. Next, the key parameters in the optimized design are selected as optimization variables,

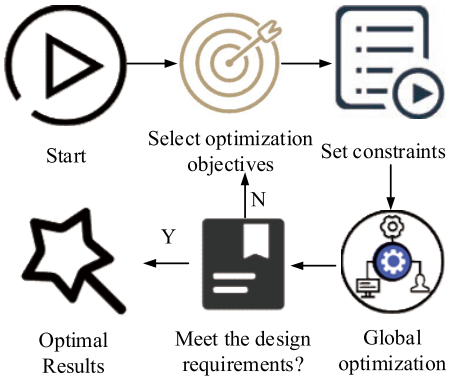

FIGURE 5. Optimized design flowchart.

and the objective function and constraints are set at the same time. Subsequently, the appropriate optimization algorithm is selected, and tools are used to perform global optimization calculations. During the optimization process, it is necessary to determine whether the design meets the requirements. If it does not satisfy the requirements, the design parameters and optimization algorithm are adjusted, and the optimization iteration is repeated. If it meets the design requirements, it will conduct a multi-indicator comparison analysis to ensure the feasibility and effectiveness of the optimization scheme. Finally, the results of the optimization design are output to form a complete optimization scheme. The study selects efficiency and PD as the optimization objectives, whose expressions are shown in Equation (7).

$$\begin{cases} \eta = \frac{P_o}{P_o+P_t} \times 100\% \\ P_d = \frac{P_o}{W_t} \end{cases} \tag{7}$$

Let P_o denote the motor output power, η the motor efficiency, P_d the PD, and W_t the effective material weight of the motor. The parameters to be optimized in the motor part are shown in Fig. 6.

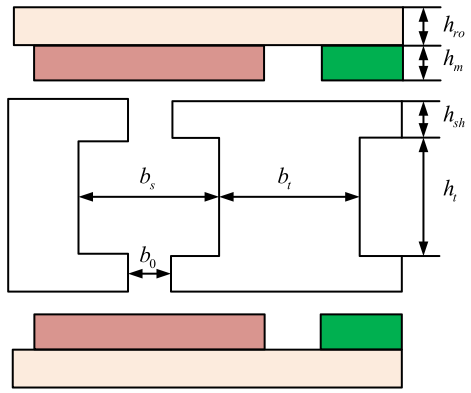

FIGURE 6. Parameters to be optimized for the motor.

In Fig. 6, h_m denotes the thickness of the PM, which determines the magnitude of magnetic flux and rotor magnetic performance; h_{ro} denotes the thickness of the outer layer of the rotor, which affects the mechanical strength and thermal performance of the rotor; h_{sh} denotes the height of the stator slots, which affects the filling factor of the windings and the electromagnetic performance of the motor; h_t denotes the height of the stator teeth, which determines the effectiveness of the magnetic circuit and the stator strength; b_s denotes the stator slot width, which affects the wiring space of the windings and the current density; b_t denotes the stator tooth width, which determines the flux distribution and the saturation characteristics of the stator magnetic circuit; b_0 denotes the slot width, which affects the AG magnetic density distribution and the harmonic characteristics of the motor. The optimization of AFPMSM is expressed as a multi-objective optimization problem that involves maximizing efficiency and power density while minimizing energy loss and failure rate. The mathematical model is established as shown in Equation (8).

$$\begin{cases} h = \frac{P_o}{P_t+P_o} \times 100\% \\ P_d = \frac{P_o}{W_t} \\ E = P_{iron} + P_{copper} + P_{friction} + P_{eddy} \\ F = f(T, B, V) \end{cases} \tag{8}$$

In Equation (8), h represents the efficiency, P_d the power density, E the energy loss, F the failure rate, T the torque, B the magnetic flux density, and V the voltage stress. The constraint conditions are shown in Equation (9).

$$\begin{cases} T_{\max} \leq 120^{\circ}\mathrm{C} \\ V \leq 400\,\mathrm{V} \\ B_{\max} \leq 1.2\,\mathrm{T} \end{cases} \tag{9}$$

In Equation (9), $T_{\max}$ represents the thermal constraint, V the voltage constraint, and $B_{\max}$ the magnetic saturation constraint. Use MOGA to solve this optimization problem. The initial population is generated based on Latin hypercube sampling to ensure diversity. The optimization process includes fitness assessment, selection, crossover, mutation, and elite retention. The optimization termination condition is that the change in Pareto front is less than 1% within 10 generations.

3. RESULTS

The first subsection sets the parameters of the GA and then compares its performance. The second subsection analyzes the effect of AFPMSM optimization.

3.1. Performance Analysis of Model Training Based on Multi-Objective GA

The CPU used for the experimental hardware configuration is Intel Core i5-13490KF. The GPU is NVIDIA Geforce GTX3080Ti with 8 GB of video memory and 16 GB of RAM. The dataset used is the PMSM Motor Design Data open dataset and IEEE open dataset. The PMSM Motor Design Data dataset contains geometrical, electrical, and performance parameters of the motor including speed, output torque, current, efficiency, power, voltage, number of pole pairs, and number of slots in the stator. The study selected Particle Swarm Optimization (PSO) and Ant Colony Optimization (ACO) as comparative algorithms. The basic principles for selecting these algorithms are as follows. PSO is a widely used swarm intelligence algorithm that simulates the social behavior of particles in a search space. It has been successfully applied to continuous optimization problems and demonstrated strong convergence in motor parameter optimization. ACO is a heuristic algorithm inspired by ant foraging behavior. It is particularly effective in discrete optimization problems, making it suitable for optimizing motor topology and structural parameters. PSO and ACO are commonly used in engineering optimization and share similarities with GA in terms of population-based search mechanisms. Comparing genetic algorithm with particle swarm algorithm and ant colony algorithm can provide a

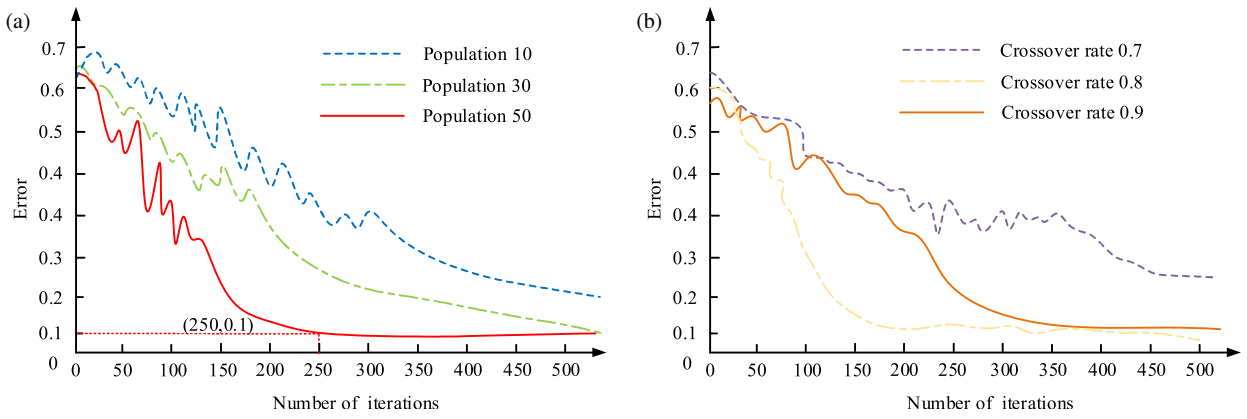

FIGURE 7. Different population sizes and crossover rates. (a) Population. (b) Crossover rate.

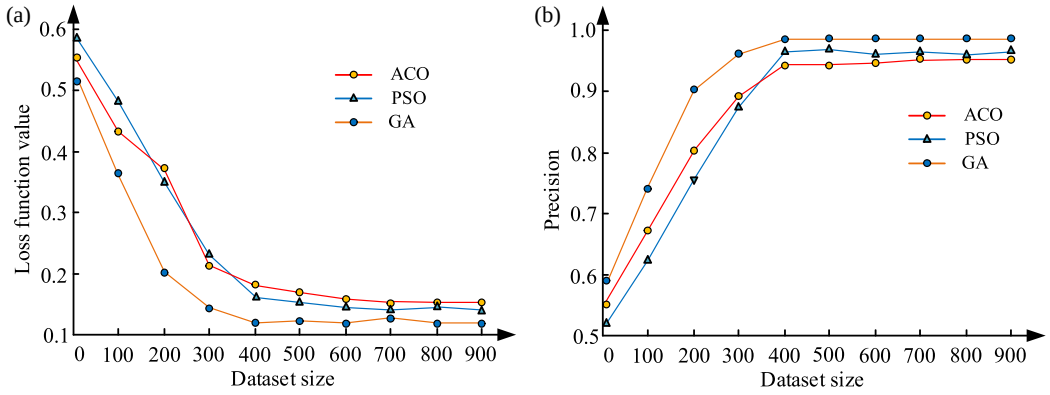

FIGURE 8. Comparison of loss functions and accuracy of each model. (a) Comparison of loss functions in the dataset size. (b) Comparison of precision in the dataset size.

deeper understanding of the advantages and disadvantages of different evolutionary and swarm intelligence based optimization strategies. The parameters of GA are first explored, and the results are shown in Fig. 7.

Figures 7(a) and 7(b) present the effect of three different population sizes (PSs) and crossover rates (CRs) on the performance of the algorithm. In Fig. 7(a), the error of the algorithm gradually decreases, and the convergence speed increases as the PS increases. Specifically, the curve with a PS of 50 is compared to PSs of 10 and 30. It shows a lower error in the early iteration stage, and the overall decreasing trend is smoother and more sustained. In Fig. 7(b), the case with a CR of 0.9 has the fastest and most pronounced decrease in error throughout the iteration. In contrast, the case with a CR of 0.7 has a smaller rate and magnitude of decline and performs the worst. This is because a higher CR promotes the mixing and transfer of superior genes, increasing the global search capability of the algorithm. GA and swarm intelligence algorithms, such as PSO and ACO, are both based on swarm optimization techniques. GA imitates natural selection, where individuals undergo crossover, mutation, and selection to evolve better solutions. The inspiration for PSO comes from social behavior in nature, where particles update their positions based on individual and global best solutions. ACO relies on pheromone updates to guide ants towards better paths, making them more suitable for combinatorial optimization problems. Unlike PSO and ACO, GA combines genetic diversity and recombination, making it more effective in exploring complex multimodal search spaces. In contrast, PSO and ACO typically converge faster, but are prone to local optima. Given these characteristics, comparing GA with PSO and ACO can help evaluate the trade-off between multi-objective motor optimization methods based on genetic evolution and swarm intelligence [18]. This allows for more efficient exploration of the solution space, which leads to faster achievement of lower errors. The low CR limits this mixing and slows down the convergence of the algorithm.

Figure 8(a) presents the change in loss function value of each algorithm as the size of the dataset increases. Fig. 8(b) presents the change in accuracy of each algorithm as the dataset size increases. In Fig. 8(a), the loss function value of GA decreases significantly with increasing dataset size and decreases most rapidly and significantly among all the algorithms. Although the loss function values of PSO and ACO also decrease with the increase of dataset size, the decrease is not as large and fast as that of GA. At dataset size of 900, the loss function value of GA is close to 0.1; the loss function value of PSO is slightly higher than 0.1; and the loss function value of ACO is around 0.15. In Fig. 8(b), GA shows the most significant improvement in accuracy over the entire range of dataset sizes and reaches a high accuracy close to 1.0 in large datasets. The accuracy of

TABLE 1. Comprehensive model performance analysis.

Model	Training error	Validation error	Final loss	Accuracy	Computation time
GA	0.05	0.08	0.10	0.98	200 ms
PSO	0.10	0.12	0.12	0.95	250 ms
ACO	0.15	0.18	0.15	0.93	300 ms
Unoptimized GA	0.20	0.25	0.30	0.8	450 ms
Model	F1 score	AUC	Recall	Precision	False positive rate
GA	0.97	0.99	0.98	0.99	0.01
PSO	0.94	0.96	0.94	0.96	0.05
ACO	0.92	0.92	0.91	0.94	0.07
Unoptimized GA	0.75	0.85	0.70	0.85	0.15

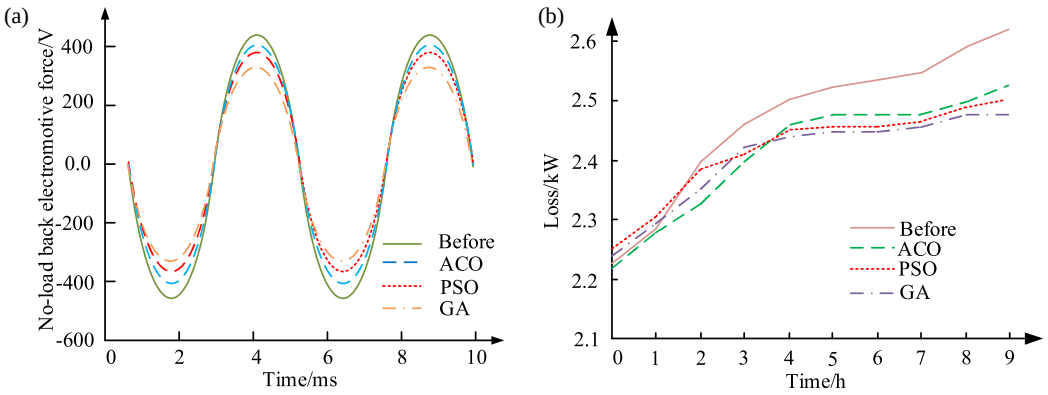

FIGURE 9. Comparison of motor line no-load back electromotive force and total loss. (a) Comparison of no-load back electromotive force of motor wires. (b) Energy loss comparison.

PSO and ACO, while also increasing with the dataset, ends up at a lower level of accuracy than GA. At a dataset size of 900, the accuracy of GA is close to 1.0, and the accuracy of PSO is slightly lower than 1.0, at around 0.95. The accuracy of ACO is also close to 0.95 but slightly lower than PSO. The suggested multi-objective GA model performs reasonably well, according to the experimental data. Each model's overall performance is examined, and Table 1 displays the findings.

In Table 1, the training error of the GA model is 0.05, and the validation error is 0.08, both significantly lower than PSO and ACO. Moreover, the final loss function value is 0.10, which is the lowest. This indicates that GA exhibits good fitting ability during the training phase. The accuracy of GA is 0.98, which is better than the 0.95 and 0.93 of PSO and ACO, while the unoptimized GA accuracy is only 0.80. GA also performs the best in terms of computation time, only requiring 200 ms, while PSO and ACO require 250 ms and 300 ms, respectively. The unoptimized GA takes the longest time, at 450 ms. The F1 score of GA is 0.97; area under the curve (AUC) is 0.99; and recall rate is 0.98. It also has advantages in these aspects, reflecting its strongest comprehensive performance in classification tasks. The F1 scores of PSO and ACO are 0.94 and 0.92, respectively, and the AUC is 0.96 and 0.92. Although the accuracy is high, the recall rate and false positive rate are relatively low. It indicates that they may not be able to effectively identify all positive class samples in certain situations. The unoptimized GA performs poorly, with an F1 score of 0.75 and an AUC of 0.85. The recall and accuracy are significantly lower than those of the optimized GA.

3.2. Analysis of AFPMSM Optimization Effects

The study uses different models to optimize the PMSM and selects the motor line no-load back electromotive force and total loss as indicators. The results are shown in Fig. 9.

Figure 9(a) presents the effect of different algorithms on the motor line no-load back electromotive force. Fig. 9(a) presents the comparison of energy losses of the motor before and after applying the algorithms. In Fig. 9(a), all the optimization algorithms reduce the fluctuation of back electromotive force. The waveforms of GA, PSO, and ACO are smoother than pre-optimization, while GA shows the least fluctuation. The peak value before optimization is about between $+400$ V and -400 V, and after optimization GA may reduce this amplitude to about $+350$ V and -350 V. In Fig. 9(b), the energy loss of the motor increases gradually after all algorithms are processed, but the optimized energy consumption is lower than that of the unoptimized state. Among them, GA exhibits the lowest energy consumption growth rate, followed by PSO and ACO. The energy consumption of the unoptimized model increases to about 2.6 kVt, and the energy consumption of the GA increases only to about 2.4 kVt. The results show that the

TABLE 2. Comprehensive performance analysis of the motor after each optimization model.

Model	Unoptimized	GA	PSO	ACO	ANSYS [19]
Efficiency (%)	85	92	90	89	87
Maximum power (kW)	200	250	240	235	233
Average energy consumption (kWh)	3	2.5	2.7	2.8	2.8
Failure rate (%)	5	1.5	2	3	1.3
Noise level (dB)	70	65	68	67	62
Energy loss (kWh)	0.5	0.3	0.35	0.38	0.42
Control stability	60	98	88	85	84
Disturbance resistance	62	99	95	84	89
Noise sensitivity	68	97	96	85	81
System response frequency (Hz)	50	100	85	80	82

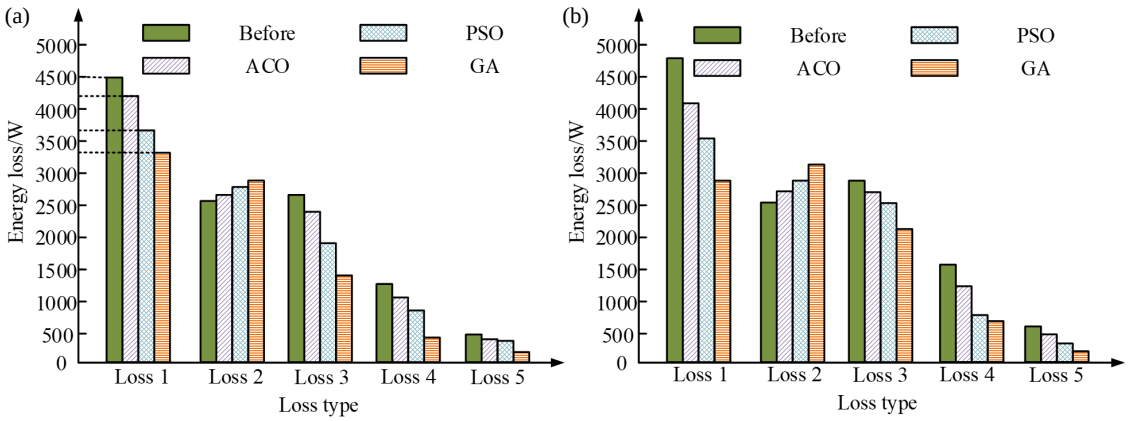

FIGURE 10. Loss analysis after optimization of each model. (a) Test 1. (b) Test 2.

proposed method exhibits high efficiency in these optimization metrics, which effectively reduces the energy consumption and the electromotive force fluctuation, and improves the overall performance of the motor. Iron consumption, copper consumption, PM eddy current loss, bearing friction loss, and air friction loss are selected as the indicators, which are named as losses 1 to 5, respectively.

Figure 10(a) presents the comparison of motor losses under different optimization algorithms in the first test. Fig. 10(b) presents the comparison of motor losses under different optimization algorithms in the second test. In Fig. 10(a), the unoptimized state has the highest loss and exhibits an energy consumption about 4500 W. After optimization, especially with GA, the losses are significantly reduced to a lower level, indicating that GA is most effective in reducing iron consumption. The energy losses under PSO and ACO are also reduced but not as significantly as those under GA. In Fig. 10(b), GA usually achieves the lowest energy loss in all loss types. The experimental results show that the optimization algorithms such as GA can significantly improve the energy efficiency of the motor, especially in reducing the critical losses such as iron loss and PM eddy current loss. The overall performance of the motor optimized by each model is analyzed, and the results are shown in Table 2.

According to Table 2, the GA optimization performs best in terms of efficiency, reaching 92%, which is significantly higher than the unoptimized 85%, indicating that the GA can effectively improve the energy efficiency of the motor and reduce the energy loss. In terms of maximum power output, GA also leads, increasing to 250 kW, which is 25% higher than the unoptimized state, reflecting the improved output capability of the motor after GA optimization. In terms of average energy consumption, GA reduces it to 2.5 kWh, which is a significant improvement compared to the unoptimized 3 kWh, indicating that the optimization algorithm effectively reduces the energy consumption during motor operation. The failure rate has decreased from 5% before optimization to 1.5% after GA optimization, indicating that the optimization significantly improves the reliability of the motor and reduces the probability of failure. The noise level has also been reduced from 70 dB to 65 dB, improving the comfort of the operating environment. The control stability, disturbance resistance, noise sensitivity, and system response frequency have also been significantly improved. Especially, under GA optimization, the control stability increases from 60 to 98, and the disturbance resistance and noise sensitivity are also close to perfect, reaching 99 and 97, respectively. Moreover, the system response frequency increases from 50 Hz to 100 Hz. They are significantly better than the model proposed by Wang et al. [19].

4. CONCLUSION

To address the design challenges of AFPMSMs in high PD and high efficiency applications, the key design parameters were investigated to be optimized by multi-objective GA. A two-dimensional equivalent model was used to perform a detailed analysis of the motor MF and armature response, which was combined with a GA for MOO to improve the efficiency and PD of the motor. The experimental results indicated that the optimized motor efficiency reached 92%, and the PD was increased by 25%. Its energy consumption was reduced to 2.5 kWh, the failure rate reduced to 1.5%, and the noise level reduced to 65 dB, which was significantly better than the traditional PSO and ACO algorithms. In addition, the GA optimization also performed well in terms of control stability, disturbance resistance, and system response frequency, which were improved to 98, 99, and 100 Hz, respectively, further verifying the advantages of GA in MOO. The research results indicated that the optimization method based on multi-objective GA could effectively enhance the comprehensive performance of AFPMSM and significantly improve its competitiveness in high PD and high efficiency applications. However, there are also some shortcomings in the research. For example, the parameter selection of optimization algorithms has a significant impact on the results, high algorithm complexity, and long computation time. Future research will focus on further optimizing the parameter settings of GA to reduce the computational complexity. By introducing automatic adjustment techniques such as Bayesian optimization, the dynamic adjustment of optimization algorithm parameters can be achieved, thereby improving the adaptability of the algorithm, reducing the dependence on manual parameter adjustment, and reducing the volatility of optimization results.

ACKNOWLEDGEMENT

The research was supported by Henan Province Demonstration Virtual Simulation Training Base for Vocational Education — Intelligent Manufacturing Virtual Simulation Training Base (No. 2023-198).

REFERENCES

[1] Peng, Z., L. Wang, L. Tong, H. Zou, D. Liu, and C. Zhang, "Multi-threshold image segmentation of 2D OTSU inland ships based on improved genetic algorithm," *PloS One*, Vol. 18, No. 8, e0290750, 2023.

[2] Kang, M., Y. Li, L. Jiao, and M. Wang, "Differential analysis of ARX block ciphers based on an improved genetic algorithm," *Chinese Journal of Electronics*, Vol. 32, No. 2, 225–236, 2023.

[3] Zhao, J., X. Liu, S. Wang, and L. Zheng, "Review of Design and control optimization of axial flux PMSM in renewable-energy applications," *Chinese Journal of Mechanical Engineering*, Vol. 36, No. 1, 45, 2023.

[4] Bouyahia, O., F. Betin, and A. Yazidi, "Fault-tolerant fuzzy logic control of a 6-phase axial flux permanent-magnet synchronous generator," *Energies*, Vol. 15, No. 4, 1301, 2022.

[5] Jiang, C., H. Liu, P. Wheeler, F. Wu, and J. Huo, "An optimized modulation for five-phase open-end winding PMSM with sliding clamped strategy," *IEEE Transactions on Industrial Electronics*, Vol. 70, No. 9, 8819–8829, 2023.

[6] Bhattacharjee, S., S. Halder, Y. Yan, A. Balamurali, L. V. Iyer, and N. C. Kar, "Real-time SIL validation of a novel PMSM control based on deep deterministic policy gradient scheme for electrified vehicles," *IEEE Transactions on Power Electronics*, Vol. 37, No. 8, 9000–9011, 2022.

[7] Tasoglu, G. and M. A. Ilgin, "A simulation-based genetic algorithm approach for the simultaneous consideration of reverse logistics network design and disassembly line balancing with sequencing," *Computers & Industrial Engineering*, Vol. 187, 109794, 2024.

[8] Kumar, B. A., B. Jyothi, A. R. Singh, M. Bajaj, R. S. Rathore, and M. B. Tuka, "Hybrid genetic algorithm-simulated annealing based electric vehicle charging station placement for optimizing distribution network resilience," *Scientific Reports*, Vol. 14, No. 1, 7637, 2024.

[9] Shen, Y., W. Xu, X. Zhang, Y. Wang, X. Xu, and Y. Luo, "Deflection control of an active beam string structure using a hybrid genetic algorithm and back-propagation neural network," *Journal of Structural Engineering*, Vol. 150, No. 3, 04024011, 2024.

[10] Li, Z., "Retracted: Neural network economic forecast method based on genetic algorithm," *IET Software*, Vol. 17, No. 4, 681–693, 2023.

[11] Gheisari, M., H. Hamidpour, Y. Liu, P. Saedi, A. Raza, A. Jalili, H. Rokhsati, and R. Amin, "Data mining techniques for web mining: A survey," in *Artificial Intelligence and Applications*, Vol. 1, No. 1, 3–10, 2023.

[12] Zhang, J., Y. Yao, W. Sun, L. Tang, X. Li, and H. Lin, "Application of the non-dominated sorting genetic algorithm II in multi-objective optimization of orally disintegrating tablet formulation," *AAPS PharmSciTech*, Vol. 23, No. 6, 224, 2022.

[13] Ou, C., J. Wang, C. Sun, Z. Hao, Y. Han, B. Xiong, L. Wang, H. Li, J. Yu, and Y. Luo, "A high-Q mid-infrared Tamm plasmon absorber using MgF_2 and Ge aperiodic tandem films designed by the genetic algorithm," *AIP Advances*, Vol. 12, No. 3, 12–21, 2022.

[14] Kumar, H., B. Gupta, P. Singh, and A. Sandhu, "Genetic algorithm-based higher-order model reduction of proton exchange membrane fuel cell," *International Journal of Energy Research*, Vol. 46, No. 15, 24 197–24 207, 2022.

[15] Yang, J., Y. Zheng, and J. Wu, "Towards sustainable production: An adaptive intelligent optimization genetic algorithm for solid wood panel manufacturing," *Sustainability*, Vol. 16, No. 9, 3785, 2024.

[16] Wang, Y.-Y., H.-B. Sun, J. Yang, S.-D. Wu, W.-M. Wang, Y.-Q. Li, and Z.-Q. Lin, "A reliability-oriented Genetic Algorithm-Levenberg Marquardt model for leak risk assessment based on time-frequency features," *Petroleum Science*, Vol. 20, No. 5, 3194–3209, 2023.

[17] Shen, Y., W. Xu, X. Zhang, Y. Wang, X. Xu, and Y. Luo, "Deflection control of an active beam string structure using a hybrid genetic algorithm and back-propagation neural network," *Journal of Structural Engineering*, Vol. 150, No. 3, 04024011, 2024.

[18] Shahsavari, A., A. Nejat, E. Climent, and S. F. Chini, "Using genetic algorithm to find the optimum piecewise superhydrophobic pattern maximizing the lift to drag ratio on a SD 7003 foil at different working conditions," *Ocean Engineering*, Vol. 278, No. 15, 114 438.1–114 438.10, 2023.

[19] Wang, S.-C., C.-T. Tang, S.-M. Huang, and S.-Y. Wang, "Simulation analysis and optimization of electromagnetic vibration and noise of permanent magnet motor," *Journal of Vibration Engineering & Technologies*, Vol. 12, No. 4, 6371–6386, 2024.